Laser operation of a Tm:Y_2O_3 planar waveguide

Jakub W. Szela, Katherine A. Sloyan,* Tina L. Parsonage, Jacob I. Mackenzie, and Robert W. Eason

Optoelectronics Research Centre, University of Southampton, Southampton, SO17 1BJ UK

*kas@orc.soton.ac.uk

Abstract: We demonstrate the first Tm-doped yttria planar waveguide laser to our knowledge, grown by pulsed laser deposition. A maximum output power of 35 mW at 1.95 μm with 9% slope efficiency was achieved from a 12 μm-thick film grown on a $Y_3Al_5O_{12}$ substrate.

OCIS codes: (140.3070) Infrared and far-infrared lasers; (140.5680) Rare earth and transition metal solid-state lasers; (220.4610) Optical fabrication; (230.7390) Waveguides, planar.

References and links

1. J. I. Mackenzie, C. Li, D. P. Shepherd, R. J. Beach, and S. C. Mitchell, "Modeling of high-power continuous-wave Tm:YAG side-pumped double-clad waveguide lasers," IEEE J. Quantum Electron. **38**, 222–230 (2002).
2. L. Fornasiero, N. Berner, B.-M. Dicks, E. Mix, V. Peters, K. Petermann, and G. Huber, "Broadly tunable laser emission from Tm:Y_2O_3 and Tm:Sc_2O_3 at 2 μm," in *Advanced Solid State Lasers* M. Fejer, H. Injeyan, and U. Keller, eds. (Optical Society of America, 1999), paper WD5.
3. V. Peters, A. Bolz, K. Petermann, and G. Huber, "Growth of high-melting sesquioxides by the heat exchanger method," J. Cryst. Growth **237-239** 879–883 (2002).
4. C. Grivas, D. P. Shepherd, T. C. May-Smith, R. W. Eason, and M. Pollnau, "Single-transverse-mode Ti:sapphire rib waveguide laser," Opt. Express **13,** 210–215 (2005).
5. C. Grivas, T. C. May-Smith, D. P. Shepherd, and R. W. Eason, "Laser operation of a low loss (0.1 $dBcm^{-1}$) Nd:$Gd_3Ga_5O_{12}$ thick (40 μm) planar waveguide grown by pulsed laser deposition," Opt. Commun. **229,** 355–361 (2004).
6. T. Gun, A. Kahn, B. Ileri, K. Petermann, and G. Huber, "Two-dimensional growth of lattice matched Nd-doped $(Gd,Lu)_2O_3$ films on Y_2O_3 by pulsed laser deposition," Appl. Phys. Lett. **93,** 053108 (2008).
7. E. R. Smith, J. B. Gruber, P. Wellenius, J. F. Muth, and H. O. Everitt, "Spectra and energy levels of Eu^{3+} in cubic phase Gd_2O_3," Phys. Status Solidi B, **247,** 1807–1813 (2010).
8. P. B. W. Burmester, G. Huber, M. Kurfiss, and M. Schilling, "Crystalline growth of cubic (Eu, Nd):Y_2O_3 thin films on α-Al_2O_3," Appl. Phys. A. **80,** 627–360 (2005).
9. A. Huignard, A. Aron, P. Aschehoug, B. Viana, J. Théry, A. Laurent, and J. Perrière, "Growth by laser ablation of Y_2O_3 and Tm:Y_2O_3 thin films for optical applications," J. Mater. Chem. **10,** 549–554 (2000).
10. S. Zhang and R. Xiao, "Yttrium oxide films prepared by pulsed laser deposition," J. Appl. Phys. **83,** 3842–3848 (1998).
11. A. K. Singh, T. R. G. Kutty, and S. Sinha, "Pulsed laser deposition of corrosion protective Yttrium Oxide (Y_2O_3) coating," J. Nucl. Mater. **420,** 374–381 (2012).
12. A. Kahn, S. Heinrich, H. Kühn, K. Petermann, J. D. B. Bradley, K. Wörhoff, M. Pollnau, and G. Huber, "Low threshold monocrystalline Nd:$(Gd, Lu)_2O_3$ channel waveguide laser," Opt. Express **17,**(6) 4112–4118 (2009).
13. H. Kühn, S. Heinrich, A. Kahn, K. Petermann, J. D. B. Bradley, K. Wörhoff, M. Pollnau, and G. Huber, "Monocrystalline Yb^{3+}:$(Gd,Lu)_2O_3$ channel waveguide laser at 976.8 nm," Opt. Lett. **34,** 2718–2720 (2009).
14. T. C. May-Smith, A. C. Muir, M. S. B. Darby, and R. W. Eason, "Design and performance of a ZnSe tetra-prism for homogeneous substrate heating using a CO_2 laser for pulsed laser deposition experiments," Appl. Optics **47,** 1767–1780 (2008).
15. O. Pons-Y-Moll, J. Perrier, E. Millon, R. M. Defourneau, D. Defourneau, B. Vincent, A. Essahlaoui, A. Boudrioua, and W. Seiler, "Structural and optical properties of rare-earth-doped Y_2O_3 waveguides grown by pulsed-laser deposition," J. Appl. Phys. **92,** 4885–4890 (2002).
16. "Inorganic Crystal Structure Database," http://icsd.cds.rsc.org/

#186939 - $15.00 USD Received 13 Mar 2013; revised 2 May 2013; accepted 3 May 2013; published 14 May 2013

17. D. E. Zelmon, D. L. Small, and R. Page, "Refractive-index measurements of undoped yttrium aluminum garnet from 0.4 to 5.0 μm," Appl. Opt. **37**(21), 4933–4935 (1998).
18. W. J. Tropf, M. E. Thomas, and E. W. Rogala, "Properties of crystals and glasses," in *Handbook of Optics, 3rd edition* M. Bass, ed. (McGraw Hill Professional, 2010).
19. S. J. Barrington, T. Bhutta, D. P. Shepherd, and R. W. Eason, "The effect of particulate density on performance of Nd:$Gd_3Ga_5O_{12}$ waveguide lasers grown by pulsed laser deposition," Opt. Commun. **185,** 145–152 (2000).
20. Y. Guyot, R. Moncorgé, L. D. Merkle, A. Pinto, B. McIntosh, and H. Verdun, "Luminescence properties of Y_2O_3 single crystals doped with Pr^{3+} or Tm^{3+} and codoped with Yb^{3+}, Tb^{3+} or Ho^{3+} ions," Opt. Mater. **5**(1-2), 127-136 (1996).
21. A. A. Anderson, C. L. Bonner, D. P. Shepherd, R. W. Eason, C. Grivas, D. S. Gill, and N. Vainos, "Low loss (0.5 dB/cm) Nd:$Gd_3Ga_5O_{12}$ waveguide layers grown by pulsed laser deposition," Opt. Commun. 144, 183–186 (1997).
22. F. S. Ermeneux, Y. Sun, R. L. Cone, R. W. Equall, R. L. Hutcheson, and R. Moncorge, "Efficient CW 2 μm Tm^{3+}:Y_2O_3 Laser," in *Advanced Solid State Lasers* M. Fejer, H. Injeyan, and U. Keller, eds.(Optical Society of America, 1999), paper TuB8.
23. J. R. Salcedo, J. M. Sousa, and V. V. Kuzmin, "Theoretical treatment of relaxation oscillations in quasi-three-level systems," Appl. Phys. B **62**, 83–85 (1996).

1. Introduction

Lasers operating in the 2 micron wavelength region have a number of applications, including remote sensing/LIDAR, materials processing and medical therapy. Thulium-doped media have several attractive features for generating light in this wavelength band, including a broad emission bandwidth, long-lived metastable states, absorption bands matched to high-power 0.8 μm diode-pump sources, and the potential for high quantum efficiency due to a 2-for-1 cross-relaxation process [1, 2]. Waveguide lasers are compact, can be easily integrated with diode pump lasers without additional beam shaping, can have lower thresholds than bulk geometries and have excellent thermal management properties. These are all features that are highly desirable in many 2 micron applications, particularly where high pump and output powers are desired.

Rare earth (RE) sesquioxides, including doped Sc_2O_3 (scandia), Y_2O_3 (yttria) and Lu_2O_3 (lutetia) are of great interest as potential waveguide laser hosts. These cubic materials have excellent thermo-optic properties and can easily be doped with various RE ions (including thulium) and are optically isotropic. Sesquioxides can, however, be challenging to grow from the melt due to their relatively high melting points (generally in excess of 2400 °C) [3].

Pulsed laser deposition (PLD) is a simple but versatile thin film deposition technique that has proven suitable for growth of low-loss lasing waveguides [4, 5]. Despite the high growth temperatures required for deposition (∼700 °C or above), growth of various sesquioxide films has been achieved via PLD [6, 7], including doped and undoped Y_2O_3 [8–11]. Lasing has been observed in Nd:$(Gd,Lu)_2O_3$ [12] and Yb:$(Gd,Lu)_2O_3$ [13] channel waveguides formed by post-processing of PLD-grown films. Estimated optical losses (propagation + unquantified coupling losses) in these latter cases have, however, been high (>4 $dBcm^{-1}$), and thicknesses limited to ∼2 μm.

In this paper we present the growth and laser operation of a 12 μm-thick Tm^{3+}:Y_2O_3 planar waveguide grown on a $Y_3Al_5O_{12}$ (YAG) substrate by PLD, representing the first example to our knowledge of a Tm:Y_2O_3 waveguide laser. Threshold pump power and slope efficiency were determined to be 135 mW and 9% respectively, leading to a maximum output power of 35 mW measured for a maximum pump power of 600 mW; this is, to our knowledge, the highest output power recorded for a sesquioxide laser grown by PLD by more than a factor of two.

#186939 - $15.00 USD Received 13 Mar 2013; revised 2 May 2013; accepted 3 May 2013; published 14 May 2013

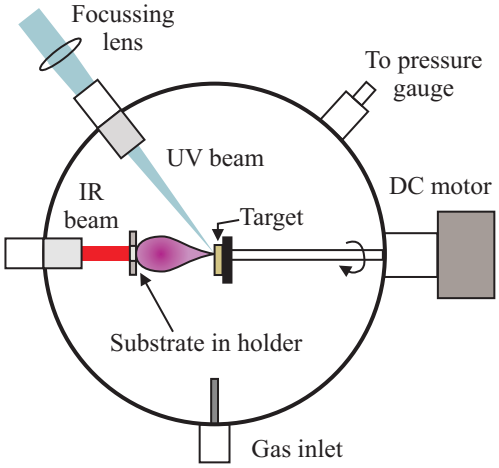

Fig. 1. Diagram of experimental setup, including UV ablating and IR heating laser beams.

2. Film fabrication and characterization

2.1. Fabrication

The ∼12 μm-thick film was deposited onto a (100)-oriented YAG substrate of size 10×10×1 mm^3 via the experimental setup displayed in Fig. 1. KrF excimer laser pulses of wavelength 248 nm, duration 20 ns and fluence 1.7 Jcm^{-2} were incident upon a Tm:doped ceramic yttria target. The substrate was heated to ∼1000 °C via a CO_2 laser of wavelength 10.6 μm, incident upon a ZnSe tetraprism to obtain a square beam profile [14]. The target was rotated, driven by an offset cam assembly, providing an epitrochoidal ablation path and hence efficient use of the target surface. Deposition took place in a background oxygen gas pressure of 4×10^{-2} mbar. Following material charaterization, two opposing facets were polished plane and parallel for lasing experiments, resulting in a final waveguide length of ∼8 mm.

2.2. Material characterization

X-ray diffraction (XRD) was carried out using a Bruker D2 Phaser powder diffractometer. XRD data was obtained for films on substrates and the bare substrates to allow peaks resulting from diffraction from the substrate to be identified. A KLA Tencor P16 stylus profiler was used to measure film thickness and a Zemetrics Zescope optical profiler was used to obtain 3D surface profile maps, allowing automatic particulate counting with the Image Metrology *Scanning Probe Image Processor* (SPIP) software package.

Energy dispersive X-ray analysis (EDX) was employed to characterize the composition of the sample. The system used was an Oxford Inca PentaFex-x3 EDX analyser attached to a Zeiss EVO-50 scanning electron microscope (SEM). The average thulium concentration in a ∼1 mm^2 area in the film center was found to be ∼2.3 at.%. Although the thulium concentration across a wider area was not measured, characterisation of previous Tm:Y_2O_3 growth under the same conditions suggests that it does not vary systematically across the entire film surface.

The film was crystalline, as was demonstrated by the XRD spectrum shown in Fig. 2(a). The largest peaks correspond to (222) and (444) orientations of the film, as well as the (400) and (800) orientations of the underlying YAG substrate, indicating that the film is highly textured in the (222) orientation. (222)-oriented growth has been observed previously in sesquioxide

#186939 - $15.00 USD Received 13 Mar 2013; revised 2 May 2013; accepted 3 May 2013; published 14 May 2013

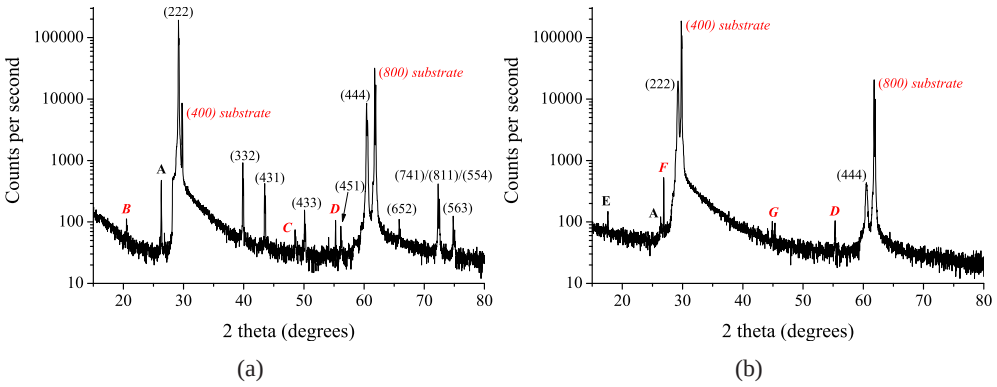

Fig. 2. XRD spectra of (a) the 12 μm-thick Tm^{3+}:Y_2O_3 waveguide and (b) a 50 nm-thick Tm^{3+}:Y_2O_3 film. Very small peaks corresponding to growth in orientations other than the primary (222) and (444) orientation can be observed, particularly in case (a). Unassigned film peaks are observed around 26.4° (A) and 17.6° (E). Peaks arising from substrate contributions may also be observed: peaks labelled B and C may correspond to orientations of cubic yttria, while peaks D, F and G likely correspond to orientations of $YAlO_3$.

deposition, both where the film and substrate were lattice matched (for example in the case of growth of yttria on sapphire, where the lattice mismatch was ∼5% [8]), and in the case of growth on amorphous substrates (where there is no lattice match, growth in the cubic phase and {111} orientation minimises the surface free energy [15]). A number of peaks at least two orders of magnitude smaller than the primary (222) orientation peak can also be observed. This indicates a small amount of growth in other orientations and possibly in a non-cubic phase (corresponding to the peak labelled A). This latter peak could not be assigned directly from database values, although a number of non-cubic orientations of Y_2O_3 exhibit peaks at a similar value of 2θ [16].

For comparison, a 50 nm Tm^{3+}:Y_2O_3 film was grown under the same deposition conditions, the XRD spectrum of which is shown in Fig. 2(b). In this case, only peaks corresponding to the (222) and (444) planes of cubic yttria can be observed, as well as additional small peaks around 17.6° (E) and 26.4° (A). This suggests that the film grows primarily in the (222) orientation even during the first tens of nanometres of growth, while growth in other orientations becomes more prevalent as the film thickness increases. A very small peak likely corresponding to the non-cubic yttria phase is also observed around 26.4°, indicating some growth in this phase even at these small thickness values.

The growth mechanisms that lead to the formation of cubic and non-cubic phases in different orientations, as well as their changing significance as film thickness increases, are currently under investigation. It should be noted that due to the small thickness of the film, the XRD spectrum is dominated by the substrate contribution, and peaks resulting from the film itself (i.e. small amounts of growth in other phases/orientations) may be lost in the noise. It should also be noted that the presence of peaks other than (400) and (800) orientations of YAG in the substrate spectra indicates that the substrates themselves are not perfect crystal, which may be influencing subsequent film growth. The peaks labelled B and C in Fig. 2(a) may correspond to the (211) and (440) orientations of cubic yttria, while peaks labelled D, F and G in Figs. 2(a) and 2(b) likely correspond to the (222), (111) and (221) orientations of $YAlO_3$ (YAP) respectively.

#186939 - $15.00 USD Received 13 Mar 2013; revised 2 May 2013; accepted 3 May 2013; published 14 May 2013

2.3. Waveguide characterization

Considering the refractive index of the YAG [17] substrate and undoped Y_2O_3 [18] (1.82 and 1.91 respectively at 800 nm), and noting that this Tm dopant concentration likely results in a negligible index increase, the numerical aperture (NA) of the waveguide at the pump and lasing wavelengths was calculated to be 0.58 and 0.57 respectively. The 12 μm-thick film should hence support up to 50 and 20 modes at the pump and laser wavelengths respectively, and is therefore a highly multi-mode structure.

Propagation losses were estimated through transmission measurements at wavelengths outside of the Tm^{3+} $^3H_4$ manifold absorption band using a tunable Ti:sapphire laser, specifically 730 nm and 850 nm. Assuming a 100% launch efficiency, the loss coefficient γ can be calculated using Eq. (1):

$$\gamma = \ln\left(\frac{P_{out}}{P_{in}(1-R)^2}\right)/l_w \tag{1}$$

where l_w is the waveguide length, R is the Fresnel reflectance at each waveguide facet and $P_{in/out}$ are the respective incident and out-coupled powers of the probe beam. For our 8 mm-long waveguide, assuming the Fresnel reflectance of pure yttria R = 9.9%, losses are estimated to be $\sim$2 dBcm^{-1} at the probe wavelengths (losses at longer wavelengths are expected to be lower due to a smaller Rayleigh scattering coefficient).

The average density of particulates of height $>$100 nm and $>$50 nm on the film surface was measured as $(9.8\pm 1.3)\times10^3$ cm^{-2} and $(15 \pm 2.4)\times10^4$ cm^{-2} respectively. Barrington et al [19] analysed the effect of particulates on propagation loss in PLD-grown laser waveguides based on films of $G_3Ga_5O_{12}$ (GGG), a cubic crystal with a similar refractive index to yttria ($\sim$1.96), grown on YAG substrates. While a direct comparison of loss values may not be valid due to the difference in material properties and growth conditions, it can still be helpful as a guide. In the GGG case, the particulate densities we have measured would be expected to result in losses of much lower than 1 dBcm^{-1}. Our estimated losses of $\sim$2 dBcm^{-1} hence suggest that particulates may not be the only source of loss in our waveguide. Other factors potentially resulting in additional scattering and subsequent loss (not quantified) include local areas of poor-quality facet polishing and strain-induced birefringence, as well as scattering at grain boundaries and/or areas of non-cubic growth. It is expected that further study of film growth mechanisms may help to explain these additional sources of loss.

To determine the optimum pump wavelength, the relative absorption spectrum of the waveguide was measured by tuning the Ti:sapphire pump laser in 0.1 nm steps across a range of 790-810 nm (see Fig. 3). The maximum absorption coefficient α was determined to be 1.45 cm^{-1} at a pump wavelength λ_p = 796.5 nm, corrected for the propagation losses determined at the out-of-band (i.e. non-absorbing) probe wavelengths, consistent with that observed in bulk crystal [2, 22]. Previously reported absorption cross section data is shown in Fig. 3 for comparison.

2.4. Spectroscopic characterization

Lifetime and emission measurements were performed at room temperature. The Tm^{3+} ions were excited to their $^3H_4$ level using the output of a fibre-coupled laser diode operating at 793 nm. The pump beam was focussed onto the face of the waveguide, perpendicular to the plane of the film and close to one edge; while the 2 μm fluorescence from the $^3F_4$ energy level, was captured as it exited the waveguide facet. At 3 W peak power and with a pump beam size at the film of 600 μm diameter, the incident irradiance was I_p = 1 kWcm^{-2}. The waveguide facet and 2 μm emission were reimaged onto a Thorlabs DET10D InGaAs detector with a germanium filter covering the active area, passing only the longer wavelength of interest. To determine the lifetime of the upper laser level the pump was modulated with 5 ms pulses at a 10% duty

#186939 - $15.00 USD Received 13 Mar 2013; revised 2 May 2013; accepted 3 May 2013; published 14 May 2013

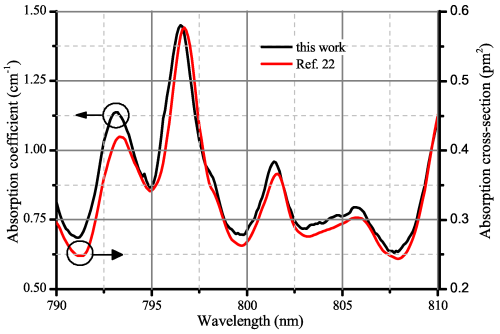

Fig. 3. Measured variation in absorption coefficient of the Tm:Y_2O_3 film with wavelength (black), with previously reported absorption cross section data for bulk crystal [22] shown for comparison (red).

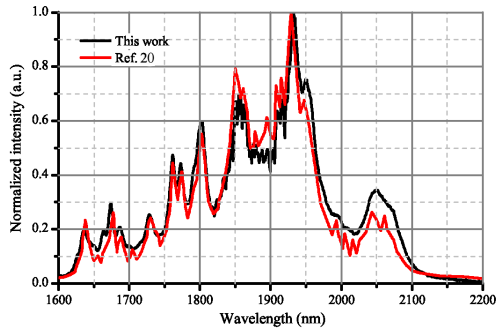

Fig. 4. Measured fluorescence emission spectrum of the Tm^{3+}:Y_2O_3 waveguide (black), with data previously observed for bulk crystal [20] shown for comparison (red).

cycle (i.e. 5 ms pulse at a period of 50 ms), enough time for the system to reach steady-state conditions.

A fluorescence lifetime of $\tau = 3.44 \pm 0.01$ ms was determined from the exponential decaying signal recorded using an Agilent MSO6104A digital oscilloscope. This is in good agreement with values reported for bulk Tm^{3+}:Y_2O_3 with lifetimes of 4.15 ms (1 at.% Tm^{3+} [2]) and 3.2 ms (2 at.% Tm^{3+} [20]). Figure 4 shows the emission spectrum measured with an ANDO AQ6375 optical spectrum analyser using a spectral bandwidth of 2 nm, along with data observed for bulk crystal [20] for comparison. The spectral profiles of waveguide and bulk are almost identical. This agreement indicates correct substitutional occupation for the thulium ions, which is not always the case for PLD grown thin films; in the case of GGG growth on YAG, for example, the spectral match between bulk and film crystal is poor due to non-stoichiometric growth and incorporation of RE ions in non-radiative sites [21].

3. Laser experiments

2 μm laser emission from the $^3F_4 \rightarrow {}^3H_6$ transition of Tm^{3+} starts with excitation into the $^3H_4$ manifold and subsequent population redistribution either by cross-relaxation or energy migration into the $^3F_4$ metastable level. The former process can provide an efficient pumping mechanism with up to two excited ions created for one pump photon, as has been exploited previously in a high-power Tm^{3+}:YAG planar waveguide laser [1]. This effect is dependent upon

#186939 - $15.00 USD Received 13 Mar 2013; revised 2 May 2013; accepted 3 May 2013; published 14 May 2013

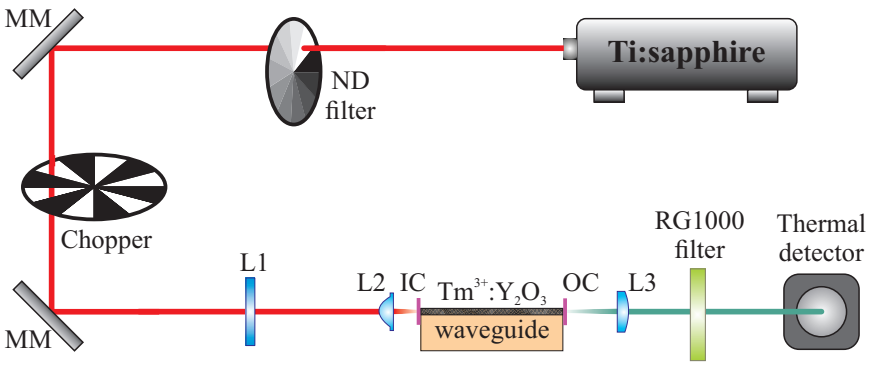

Fig. 5. Setup of the Tm^{3+}:Y_2O_3 waveguide lasing experiments. Abbreviations are as follows: MM – metal mirror; L1 – in-plane collimating cylindrical lens; L2 – aspheric lens; IC – input coupling mirror; OC – interchangeable output coupling mirror; L3 – collection lens.

the proximity of the Tm^{3+} to neighbouring dopant ions, hence the higher RE ion concentration for yttria per atomic substitution (compared to YAG) should enable sufficient cross-relaxation rates at lower doping levels as reportedly used in early bulk crystal experiments [22].

The experimental setup of the end-pumped laser is depicted in Fig. 5. It consists of a tunable Ti:sapphire pump laser, a 100 mm focal length cylindrical lens, an 11 mm focal length aspheric lens, a thin pump input coupling mirror (IC), the waveguide, and various interchangeable bulk output coupling mirrors (OC). A collection lens (NA = 0.16) was used after the output coupling mirror to transfer the 2 μm light to a thermal detector covered by a 3 mm-thick longpass filter to reject the transmitted pump light.

The near-diffraction-limited pump source was tuned to match the maximum absorption peak around 797 nm and its optical power set by a variable metallic neutral density filter, providing a maximum incident power of 600 mW after the variable filter. In the waveguide's fast-axis (guiding direction), the incident pump light was focused down to a waist of 3.6 μm at the input facet, significantly smaller than half the thickness of the active layer. The NA of the input pump lens was 0.25, much less than the acceptance NA of the waveguide, hence our assumption for a 100% launch efficiency (neglecting interface reflections). In the other (unguided) direction the beam was either collimated, with a beam waist of 90 μm positioned approximately midway along the waveguide, or diverging from the pump focus at the input facet i.e. a beam waist of 3.6 μm. The former configuration, achieved by placing the cylindrical lens before the input coupling aspheric, provided a good overlap between the pump beam width and cavity mode in the unguided axis throughout the whole waveguide. The latter configuration, however, provided higher inversion density at the input facet, at the expense of the overlap efficiency: the pump beam radius spread to ∼350 μm at the exit facet of the waveguide (calculated assuming no lensing effects in the plane), and was hence significantly larger than the ∼75 μm-radius cavity mode.

A quasi-monolithic optical resonator was made by butt-coupling plane parallel mirrors to the uncoated waveguide facets with a Fluorinert FC-70 fluid interface for the thin mirrors, holding them in place and acting as an index matching fluid. Four different OCs were investigated in total, with reflectance values of ∼99.5%, 94%, 90% and 85% at the laser wavelength. The pump transmittance of the HR IC was 92% and each of the other mirrors also had high transmission at this wavelength, leading to a single pass of the pump light. The waveguide was fixed to an aluminium pedestal on a 3-axis translation stage and was not actively cooled.

#186939 - $15.00 USD Received 13 Mar 2013; revised 2 May 2013; accepted 3 May 2013; published 14 May 2013

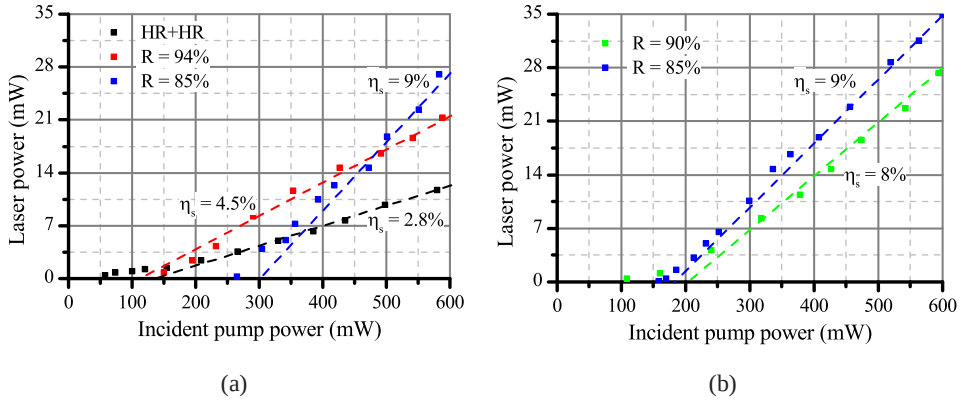

Fig. 6. Laser output power versus incident pump power for configuration (a) collimated in-plane pump (aspheric and cylindrical coupling lenses), and (b) diverging in-plane pump (single aspheric coupling lens).

Laser action was observed for both pump configurations, with the respective performance shown in Fig. 6. Despite an emission cross section that extends out to 2.1 μm [2], in all cases a laser wavelength of ∼1950 nm was observed, consistent with that reported for bulk crystal experiments [22]. This is due to the fact that the terminating laser level is in the ground-state, and the effective gain is dependent upon the difference between the emission and absorption cross sections at the lasing wavelength. Due to the relatively high gains required to overcome the losses in our system, and given that an effective inversion between the ground and upper laser level, β, of greater than 12% favours the shorter wavelengths [22], it is clear why this wavelength is observed for this system; it should be noted that for β >20% the emission wavelength would most likely switch to ∼1933 nm, where the strongest emission cross section occurs [22].

With a HR+HR cavity the lowest observed laser threshold in the first configuration was 50 mW. Higher output power was achieved in the second configuration with only the aspheric input coupling lens, as can be seen in Fig. 6(b). A maximum output power was obtained with the 85% reflective OC, with 35 mW measured for 600 mW of incident pump power with a slope efficiency of ∼9%. The same slope efficiency was observed for the lowest reflectance OC in both configurations. A scanning slit beam profiler (Datarays Beam Scope P8, InAs detector with a single 5 μm slit width), horizontally and vertically matched to the generated laser beam, was used to estimate the beam quality parameter (M^2) in the guided direction. A value of 5 ± 2.9 was obtained at full laser power.

Optical round trip losses were estimated by measuring the relaxation oscillation (RO) frequency as a function of the pump power with respect to the threshold power, including reabsorption at the laser wavelength [23]. The experimental setup was similar to Fig. 5, but with the addition of a mechanical chopper placed before the input coupling lenses. The thermal detector was replaced by a biased InGaAs detector connected to a digital oscilloscope.

For a system with reabsorption losses, the RO angular frequency ω_{RO} is given by Eq. (2) [23]:

$$\omega_{RO}^2 = \gamma_c \gamma_\tau \left(1 + \frac{N\sigma_{al} c}{n\gamma_c}\right)\left(\frac{P_p}{P_{pth}} - 1\right) \tag{2}$$

where γ_c is the cavity decay rate, γ_τ is the fluorescence decay rate, P_p is the pump power, P_{th} is the threshold pump power, N is thulium concentration, σ_{al} is the absorption cross section at the laser wavelength, c is the speed of light in vacuum, and n is the refractive index of the active medium at the laser wavelength. The loss L is obtained from the gradient of the linear fit to the

#186939 - $15.00 USD Received 13 Mar 2013; revised 2 May 2013; accepted 3 May 2013; published 14 May 2013

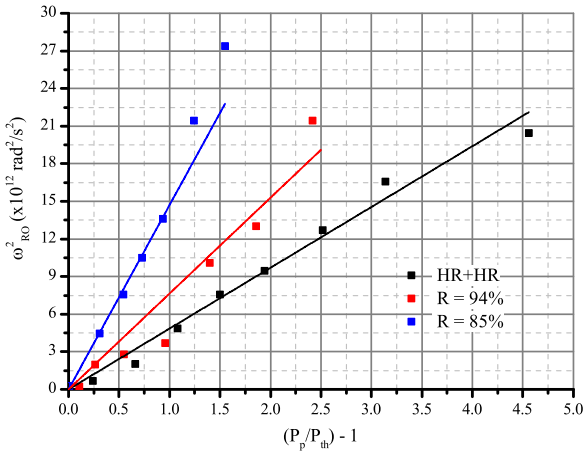

Fig. 7. Round trip cavity losses as determined via the measured relaxation oscillations

RO angular frequencies, as per Eq. (2) and shown in Fig. 7, through the cavity decay rate γ_c, and other physical parameters via Eq. (3):

$$L = 1 - \frac{1}{R_{in}R_{out}\exp\left(\frac{2\gamma_c l_{opt}}{c}\right)} \tag{3}$$

where R_{in} and R_{out} are reflectance values for the IC and OC mirrors and l_{opt} is the optical path length of the cavity. A round trip loss value of L = 5.8 $\pm$ 0.7 dB was obtained for the HR+HR cavity, highlighting that additional losses were incurred at the mirror/facet interfaces in comparison to the simple propagation losses measurement in section 2.3. Even higher round trip losses were obtained for the bulk OCs, a consequence of the small gap between the waveguide facet and mirror.

4. Conclusion

In summary, we have demonstrated the first Tm-doped yttria planar waveguide laser to our knowledge, grown by PLD. A maximum output power of 35 mW at 1.95 μm was achieved with a 9% slope efficiency. The 12 μm-thick film was highly textured in the {111} orientation with an average particulate density of (9.8 $\pm$ 1.3)$\times 10^3$ cm^{-2} (particulates of height >100 nm). Moderate propagation and mirror coupling losses currently limit the performance, as there was no sign of roll-over in the power curve even at the relatively high pump power densities investigated without any active cooling. Further improvement in performance is expected with improved film quality and direct coating of the waveguide end-facets, opening up a range of potential 2 μm high power applications from these compact gain modules.

Acknowledgments

This work has been funded under EPSRC grants EP/J008052/1 and EP/H005412/1. K.A. Sloyan acknowledges the support of an EPSRC Doctoral Prize, while T.L. Parsonage and J.W. Szela acknowledge the support of EPSRC studentships. J.W. Szela also acknowledges the support of Laser Quantum Ltd.

#186939 - $15.00 USD Received 13 Mar 2013; revised 2 May 2013; accepted 3 May 2013; published 14 May 2013